www.sciencemag.org/content/352/6291/1341/suppl/DC1

Supplementary Materials for

Zebrafish models of idiopathic scoliosis link cerebrospinal fluid flow defects to spine curvature

D. T. Grimes,* C. W. Boswell,* N. F. C. Morante,* R. M. Henkelman, R. D. Burdine, B. Ciruna†

*These authors contributed equally to this work.
†Corresponding author. Email: ciruna@sickkids.ca

Published 10 June 2016, *Science* **352**, 1341 (2016)
DOI: 10.1126/science.aaf6419

This PDF file includes:

Other Supplementary Material for this manuscript includes the following:
(available at www.sciencemag.org/content/352/6291/1341/suppl/DC1)

Movies S1 to S6

Materials and Methods

Animal Care

Established zebrafish husbandry protocols were adhered to and all protocols were performed in accordance with Canadian Council on Animal Care (CCAC) guidelines and the guidelines of the Princeton University Institutional Animal Care and Use Committee (IACUC). Wild-type zebrafish from the AB, WIK, PWT, and TL strains were used. Mutant *ptk7* (*hsc9*), *c21orf59*^{TS} (*kur*, *tm304*), *ccdc40* (*lok*, *t0237b*), and *ccdc151* (*fld*, *ts272*) lines have been described previously(*8, 20, 21, 24*). The *dyx1c1*^{pr13} line was generated by CRISPR/Cas9-mediated mutagenesis. Embryos obtained from natural matings were grown at 28^{o}C unless otherwise indicated (*31*). Scoliotic fish tested negative for the presence of potential pathogens that might induce spinal defects, including *Mycobacterium* and *Pseudoloma.*

Molecular Cloning

For RNA expression constructs, full-length ORFs of *ccd151*, *dyx1c1* and *ccdc40* were amplified from 24 hpf zebrafish cDNA generated by SuperScript IV following manufacturers instructions. Amplified products were cloned via Gateway technology (Life Technologies) into pDONR221 and subsequently shuttled into pCS2+ as expression vectors. For mRNA production, vectors were linearized with NotI and *in vitro* transcribed using mMessage mMachine SP6 kit (Ambion).

Transgenesis

-5.2*foxj1a* was amplified from zebrafish genomic DNA using GoTaq Long PCR Master Mix (Promega) using primers: forward 5'-GGGGACAACTTTGTATAGAAAAGTTGTAGCTGTATCCCATCTAGACTTTATCT-3' and reverse 5'-GGGGACTGCTTTTTTGTACAAACTTGCAAATCCTAACAGGCAGAAACATTTA-3'. The PCR product was gel purified followed by BP recombination into pDONRP4P1r (Invitrogen) to generate p5E-foxJ1aP. Entry plasmids were shuttled into standard Tol2 kit Gateway-compatible vectors (*32*) via LR recombination to generate final transgenes. Embryos were injected at the one cell stage with 25 pg plasmid and 25 pg Tol2 transposase RNA and screened at 72 hpf for transgenesis marker expression. Embryos showing strong fluorescence were sorted, grown to adulthood and individuals were crossed to wild-type AB to generate independent stable F1 lines. Imaging of GFP reporter line was performed on an Axio Zoom.V16 (Zeiss).

CRISPR/Cas9 mutagenesis

Single guide RNAs (sgRNAs) with the *dyx1c1* targeting sequencing 5'-GGAGAGGAATTCAGAAGAGGA-3', and Cas9 RNA were generated as previously described (*33*). 100 pg of sgRNA and 150 pg of Cas9 RNA were injected into the single cell of the 1-cell stage embryo. Potential mosaic fish were raised, intercrossed, and resulting embryos were screened for curved body axis at 1-3 dpf. Non-phenotypic siblings were raised and outcrossed to generate homogeneous founder lines that were sequenced (Genewiz, Inc.) for *dyx1c1* indels.

Morpholino oligonucleotide (MO) knock-down and mRNA rescue injection

Antisense MOs (GeneTools LLC) targeting *dyx1c1* or *ccdc151* were injected into the yolk of the 1-cell staged embryo. For *dyx1c1*, 2 ng of an AUG MO were injected whilst 8 ng of AUG MO targeting *ccdc151* were used(*21, 22*). For rescue injections, mRNA for zebrafish *dyx1c1* (500 pg), *ccdc40* (100 pg), and *ccdc151* (50 pg) was generated using mMESSAGE mMACHINE kits (Ambion) from full-length cloned cDNA and injected into the single cell of the 1-cell staged embryos.

Bone preparation

Zebrafish adults were fixed in 4% paraformaldehyde (PFA) in PBS for 4 days at 4°C then washed twice for 2 hours in PBS with 0.1% Tween-20. Alizarin Red and Alcian Blue staining was performed as previously described (*4*) and scales were removed manually with forceps.

μCT

Adult zebrafish were fixed in 10% neutral-buffered formalin (Sigma) overnight at 4°C. Fixed specimens were mounted in 1% low-melt agarose (Sigma) in a plastic vial. Samples were scanned for 1 h using SkyScan1172 high resolution Micro-CT scanner (Bruker micro-CT, Belgium) with the X-ray power at 45 kVp and 218 mA. All three-dimensional Micro-CT data sets were reconstructed with 18 μm isotropic resolution. Images were then analyzed using Amira software (TGS Inc., Berlin, Germany).

Scanning Electron Microscopy (SEM)

Adults were decapitated and brains were removed from the skull and surrounding tissue. Isolated whole brains were sliced in the sagittal plane along the midline and fixed in 2% glutaraldehyde in 0.1M sodium cacodylate buffer (pH 7.3) overnight at 4°C. Samples were then rinsed in 0.1M sodium cacodylate buffer with 0.2M sucrose (pH 7.3) and gradually dehydrated in an ethanol gradient. The samples were critical point dried in a Bal-tec CPD030 critical point dryer, mounted on aluminum stubs, gold coated in a Denton Desk II sputter coater and imaged on an FEI XL30 SEM (Philips).

Calcein staining

Zebrafish larvae were incubated in 0.15% Calcein (Sigma) for 10 minutes, rinsed and then washed twice for 5 minutes in system water. Larvae were immobilized in 0.005% Tricaine (Sigma), mounted in 0.8% low melting temperature agarose and imaged using a Leica M205FA microscope with a DFC365 FX camera attachment (Leica Microsystems).

Ventricle flow analysis

Whole mount adult brains were prepared fresh by dissection and washed several times with PBS before incubating in pre-warmed high glucose DMEM (Life Technologies). Brains were mounted in 1% low melt agarose prepared in DMEM and dissected using glass capillary needles to reveal the floorplate region of the rhombencephalic ventricle. A solution of 2.5% glycerol/0.2% red microspheres (1 μm, Polysciences) was loaded into a glass micropipette and the bead solution was deposited into the anterior region of the dissection. Movement of beads was captured using an

ORCA-Flash 4.0 camera (Hamamatsu). Trajectories of bead movement was tracked over 50 frames (10 seconds) using 'Temporal-Color Coder' plugin for Fiji (Kota Miura, EMBL, Heidelberg). Speeds of individual beads were measured using Imaris software (Bitplane). Means and standard error mean of bead speeds were determined using GraphPad Prism (GraphPad Software). Means between groups were compared using using a two-tailed *t*-test.

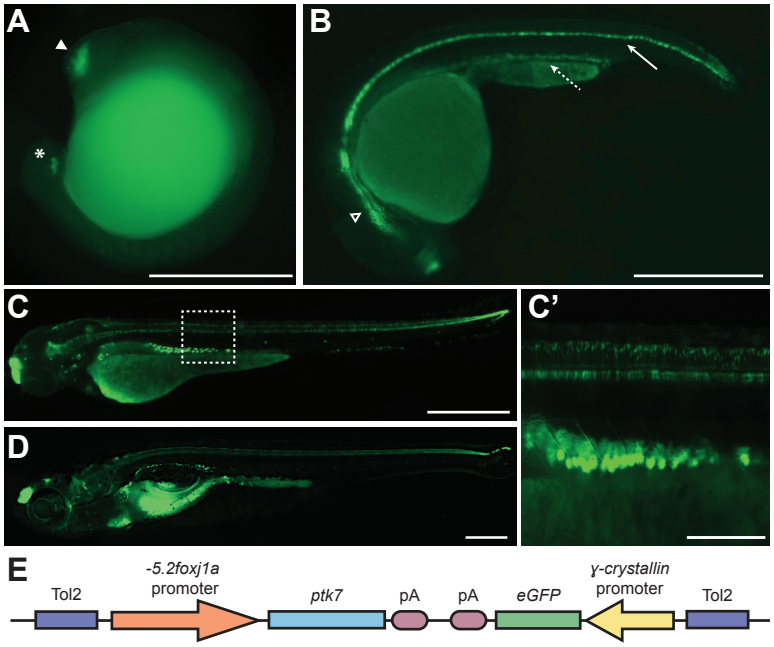

Fig. S1. ***foxj1a*** **enhancer element drives expression specifically in motile ciliated cell lineages.** (**A-D**) Tg(*foxj1a*::*eGFP*) transgenic embryos demonstrate faithful reporter expression in known motile ciliated cell lineages. Earliest GFP expression is detected during somitogenesis (A) in Kupffer's vesicle (asterisk) and olfactory pits (arrowhead). By 28 hpf (B) expression is observed within brain ventricles (empty arrowhead), pronephric ducts (dotted arrow) and neural tube floor plate (solid arrow). Transgene expression persists after organogenesis at 60hpf (C and C') and is maintained in motile ciliated tissues throughout adolescence (17 dpf) (D). (**E**) Schematic of Tg(*foxj1a*::*ptk7*) rescue transgene. Scale bars: 500 µm (A-C and D) and 250 µm (C')

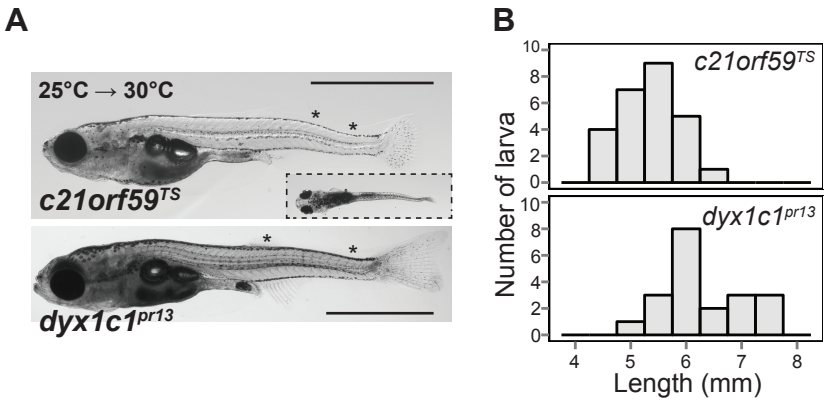

Fig. S2. Spinal curves develop during late larval stages in cilia motility mutants. (**A**) Lateral view of larval *c21orf59*^{TS} (rescued by temperature shift) and *dyx1c1*^{pr13} mutants (rescued by RNA injection) exhibiting spinal curves (asterisks). Inset shows top view of *c21orf59*^{TS} mutant. (**B**) Quantification of length of curve onset for *c21orf59*^{TS} and *dyx1c1*^{pr13} mutants illustrating the distribution data. Both mutants exhibited curves no earlier than 4.5-5 mm. Scale bar: 1 cm (A).

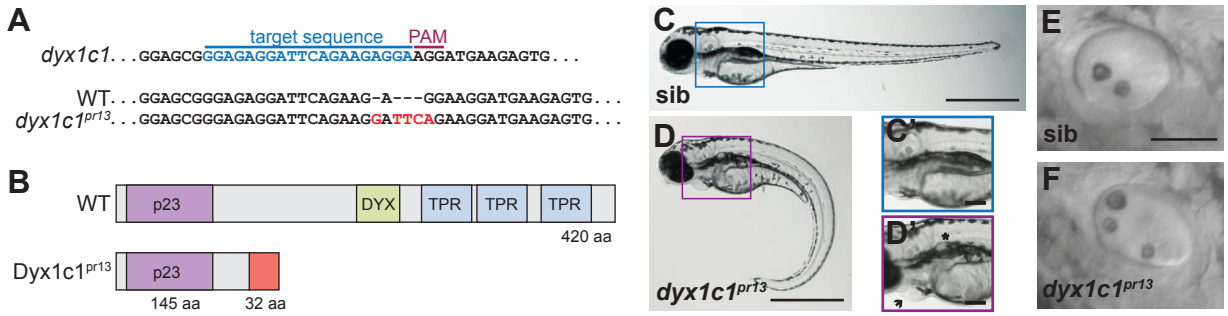

Fig. S3. Generation of *dyx1c1* mutants via CRISPR/Cas9. (**A**) Segment of the zebrafish *dyx1c1* sequence showing single guide RNA target sequence and the protospacer adjacent motif (PAM). CRISPR/Cas9-mediated mutagenesis induced an indel that caused a frame shift mutation. The line harboring this mutation was designated *dyx1c1*^{pr13}. (**B**) Schematic of the wild-type (WT) and Dyx1c1^{pr13} protein. After the frame shift at R146, 32 out-of-frame amino acids are incorporated before a premature termination codon truncates the protein. (**C-D'**) *dyx1c1*^{pr13} mutants at 3 dpf exhibited ventral body curvature (D) and kidney cysts, marked by an asterisk (D'), which were not present in sibling (sib) controls (C-C'). The arrow highlights pericardial edema, which was occasionally present in *dyx1c1*^{pr13} mutants (D'). (**E** and **F**) Lateral views of otic vesicles showing two otoliths in sib controls but abnormal numbers and positioning in *dyx1c1*^{pr13} mutants ($p=8.2\times10^{-7}$, *chi-squared test*). Scale bars: 1 mm (C and D), 0.2 mm (C' and D'), and 0.05 mm (E and F).

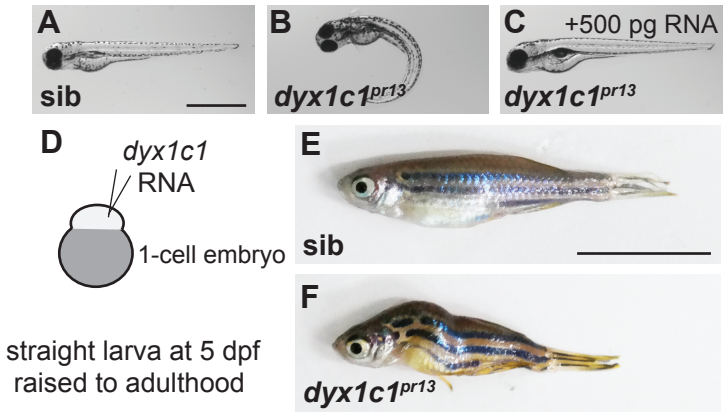

Fig. S4. *dyx1c1*^{pr13} mutants exhibit late-onset spinal curves. (**A** and **B**) Intercrosses between *dyx1c1*^{pr13} heterozygotes produced phenotypically normal siblings (sib) (A) and mutant embryos exhibiting cilia motility-associated abnormalities including ventral axis curvature at 3 dpf (B). (**C** and **D**) Injection of wild-type *dyx1c1* RNA at the 1-cell stage (D) fully rescued the embryonic phenotypes of *dyx1c1*^{pr13} mutants (C). (**E** and **F**) *dyx1c1*^{pr13} mutants rescued by RNA injection and then raised to sexual maturity exhibited late-onset spinal curves (F) whereas sib controls did not (E). Scale bars: 1 mm (A), and 1 cm (E).

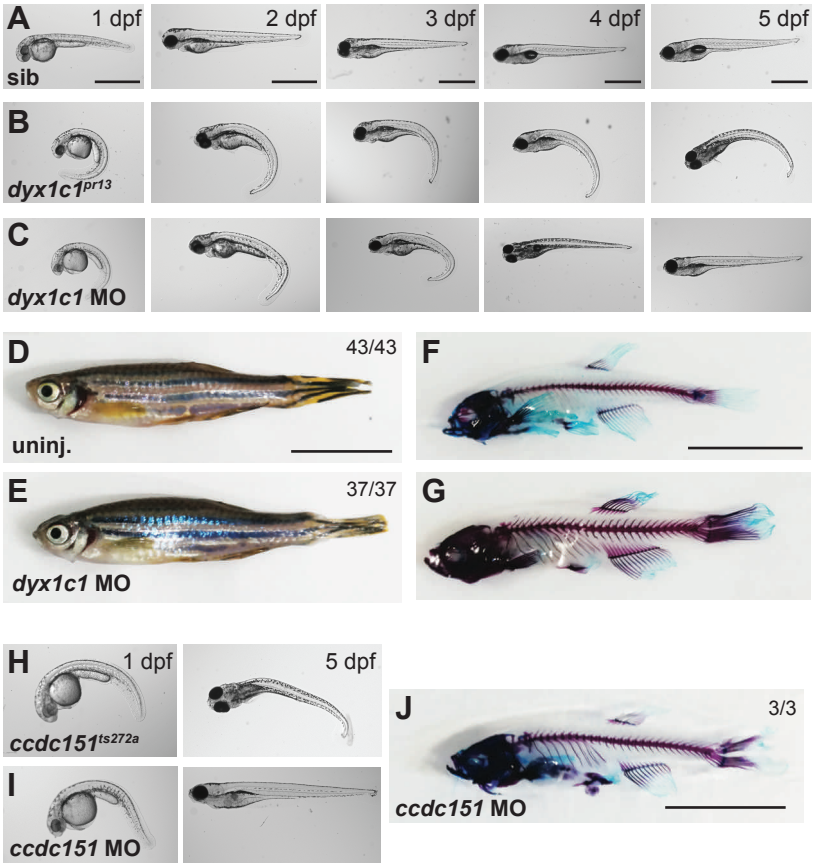

Fig. S5. Knock-down of cilia motility genes during embryonic development does not cause late-onset spinal curves. (**A-C**) The first 5 days of embryonic development in sibling (sib) controls (A), *dyx1c1*^{pr13} mutants (B), and embryos injected at the 1-cell stage with *dyx1c1* antisense morpholino oligonucleotides (MO) to knock-down Dyx1c1 expression (C)**.** Whilst both mutants and morphants exhibited early ventral axis curvature, morphants were able to recover from this defect by 5 dpf likely owing to reduced effectiveness of the MO as the embryo enlarges. Mutants, by contrast, cannot recover from ventral axis curvature. (**D-G**) Lateral views of uninjected control (uninj.) and *dyx1c1* morphants at sexual maturity with Alizarin Red and Alcian Blue staining (F-G) showing an absence of spinal curves in morphants that had exhibited ventral axis curvature as embryos. (**H** and **I**) Whereas *ccdc151* mutants exhibit ventral axis curvature throughout embryonic stages (H), transient knock-down of *ccdc151* by MO resulted in ventral axis curvature which recovered by 5 dpf (I). (**J**) Alizarin Red and Alcian Blue staining revealed an absence of spinal curves in *ccdc151* morphants. Scale bars: 1 mm (A,B,C), and 1 cm (D,F,J).

Movie S1: Microsphere bead flow and CSF dynamics within the *ptk7/+* rhombencephalic ventricle. 50 frames = 10 seconds.

Movie S2: Microsphere bead flow and CSF dynamics within the *ptk7* mutant rhombencephalic ventricle. 50 frames = 10 seconds.

Movie S3: *foxj1a* enhancer element drives gene expression within the midline of the brain and spinal cord. Three-dimensonal reconstruction of a z-series through the trunk and neural tube of a 48hpf Tg(*foxj1a::eGFP*) embryo revealing eGFP fluorescence in the dorsal roof plate and ventral floor plate.

Movie S4: Microsphere bead flow and CSF dynamics within *ptk7* + Tg(*foxj1a::ptk7*) zebrafish rhombencephalic ventricle. 50 frames = 10 seconds.

Movie S5: Microsphere bead flow and CSF dynamics within the *c21orf59^{TS}* mutant rhombencephalic ventricle. Live imaging movie showing flow of fluorescent microspheres in 10 seconds. Tissue was maintained at 30°C for the duration of the dissection and imaging.

Movie S6: Rescued *c21orf59^{TS}* mutant zebrafish model idiopathic scoliosis. Three-dimensional microCT reconstruction (18 μm isotrophic resolution) of an adult *c21orf59^{TS}* mutant zebrafish, which was raised through the first 5 days of embryonic development at permissive temperatures (25°C) before being shifted to a restrictive temperature of 30°C.

References and Notes

1. J. C. Cheng, R. M. Castelein, W. C. Chu, A. J. Danielsson, M. B. Dobbs, T. B. Grivas, C. A. Gurnett, K. D. Luk, A. Moreau, P. O. Newton, I. A. Stokes, S. L. Weinstein, R. G. Burwell, Adolescent idiopathic scoliosis. *Nat. Rev. Dis. Prim.* **1**, 15030 (2015). doi:10.1038/nrdp.2015.30

2. M. M. Janssen, R. F. de Wilde, J. W. Kouwenhoven, R. M. Castelein, Experimental animal models in scoliosis research: A review of the literature. *Spine J.* **11**, 347–358 (2011). Medline doi:10.1016/j.spinee.2011.03.010

3. K. F. Gorman, F. Breden, Idiopathic-type scoliosis is not exclusive to bipedalism. *Med. Hypotheses* **72**, 348–352 (2009). Medline doi:10.1016/j.mehy.2008.09.052

4. M. Hayes, X. Gao, L. X. Yu, N. Paria, R. M. Henkelman, C. A. Wise, B. Ciruna, *ptk7* mutant zebrafish models of congenital and idiopathic scoliosis implicate dysregulated Wnt signalling in disease. *Nat. Commun.* **5**, 4777 (2014). Medline doi:10.1038/ncomms5777

5. J. G. Buchan, R. S. Gray, J. M. Gansner, D. M. Alvarado, L. Burgert, J. D. Gitlin, C. A. Gurnett, M. I. Goldsmith, Kinesin family member 6 (kif6) is necessary for spine development in zebrafish. *Dev. Dyn.* **243**, 1646–1657 (2014). Medline doi:10.1002/dvdy.24208

6. S. A. Patten, P. Margaritte-Jeannin, J. C. Bernard, E. Alix, A. Labalme, A. Besson, S. L. Girard, K. Fendri, N. Fraisse, B. Biot, C. Poizat, A. Campan-Fournier, K. Abelin-Genevois, V. Cunin, C. Zaouter, M. Liao, R. Lamy, G. Lesca, R. Menassa, C. Marcaillou, M. Letexier, D. Sanlaville, J. Berard, G. A. Rouleau, F. Clerget-Darpoux, P. Drapeau, F. Moldovan, P. Edery, Functional variants of *POC5* identified in patients with idiopathic scoliosis. *J. Clin. Invest.* **125**, 1124–1128 (2015). Medline doi:10.1172/JCI77262

7. S. Sharma, D. Londono, W. L. Eckalbar, X. Gao, D. Zhang, K. Mauldin, I. Kou, A. Takahashi, M. Matsumoto, N. Kamiya, K. K. Murphy, R. Cornelia, TSRHC Scoliosis Clinical Group, Japan Scoliosis Clinical Research Group, J. A. Herring, D. Burns, N. Ahituv, S. Ikegawa, D. Gordon, C. A. Wise, A *PAX1* enhancer locus is associated with susceptibility to idiopathic scoliosis in females. *Nat. Commun.* **6**, 6452 (2015). Medline doi:10.1038/ncomms7452

8. M. Hayes, M. Naito, A. Daulat, S. Angers, B. Ciruna, Ptk7 promotes non-canonical Wnt/PCP-mediated morphogenesis and inhibits Wnt/β-catenin-dependent cell fate decisions during vertebrate development. *Development* **140**, 1807–1818 (2013). Medline doi:10.1242/dev.090183

9. T. J. Park, B. J. Mitchell, P. B. Abitua, C. Kintner, J. B. Wallingford, Dishevelled controls apical docking and planar polarization of basal bodies in ciliated epithelial cells. *Nat. Genet.* **40**, 871–879 (2008). Medline doi:10.1038/ng.104

10. A. Borovina, S. Superina, D. Voskas, B. Ciruna, Vangl2 directs the posterior tilting and asymmetric localization of motile primary cilia. *Nat. Cell Biol.* **12**, 407–412 (2010). Medline doi:10.1038/ncb2042

11. A. Caron, X. Xu, X. Lin, Wnt/β-catenin signaling directly regulates Foxj1 expression and ciliogenesis in zebrafish Kupffer's vesicle. *Development* **139**, 514–524 (2012). Medline doi:10.1242/dev.071746

12. V. Singla, J. F. Reiter, The primary cilium as the cell's antenna: Signaling at a sensory organelle. *Science* **313**, 629–633 (2006). Medline doi:10.1126/science.1124534

13. S. C. Goetz, K. V. Anderson, The primary cilium: A signalling centre during vertebrate development. *Nat. Rev. Genet.* **11**, 331–344 (2010). Medline doi:10.1038/nrg2774

14. J. J. Essner, K. J. Vogan, M. K. Wagner, C. J. Tabin, H. J. Yost, M. Brueckner, Left–right development: Conserved function for embryonic nodal cilia. *Nature* **418**, 37–38 (2002). Medline doi:10.1038/418037a

15. M. J. Simon, J. J. Iliff, Regulation of cerebrospinal fluid (CSF) flow in neurodegenerative, neurovascular and neuroinflammatory disease. *Biochim. Biophys. Acta* **1862**, 442–451 (2016). Medline doi:10.1016/j.bbadis.2015.10.014

16. L. Lee, Riding the wave of ependymal cilia: Genetic susceptibility to hydrocephalus in primary ciliary dyskinesia. *J. Neurosci. Res.* **91**, 1117–1132 (2013). Medline doi:10.1002/jnr.23238

17. W. J. Wang, H. Y. Yeung, W. C. Chu, N. L. Tang, K. M. Lee, Y. Qiu, R. G. Burwell, J. C. Cheng, Top theories for the etiopathogenesis of adolescent idiopathic scoliosis. *J. Pediatr. Orthop.* **31**, S14–S27 (2011). Medline doi:10.1097/BPO.0b013e3181f73c12

18. V. G. Engesaeth, J. O. Warner, A. Bush, New associations of primary ciliary dyskinesia syndrome. *Pediatr. Pulmonol.* **16**, 9–12 (1993). Medline doi:10.1002/ppul.1950160103

19. S. P. Choksi, G. Lauter, P. Swoboda, S. Roy, Switching on cilia: Transcriptional networks regulating ciliogenesis. *Development* **141**, 1427–1441 (2014). Medline doi:10.1242/dev.074666

20. A. Becker-Heck, I. E. Zohn, N. Okabe, A. Pollock, K. B. Lenhart, J. Sullivan-Brown, J. McSheene, N. T. Loges, H. Olbrich, K. Haeffner, M. Fliegauf, J. Horvath, R. Reinhardt, K. G. Nielsen, J. K. Marthin, G. Baktai, K. V. Anderson, R. Geisler, L. Niswander, H. Omran, R. D. Burdine, The coiled-coil domain containing protein CCDC40 is essential for motile cilia function and left-right axis formation. *Nat. Genet.* **43**, 79–84 (2011). Medline doi:10.1038/ng.727

21. R. Hjeij, A. Onoufriadis, C. M. Watson, C. E. Slagle, N. T. Klena, G. W. Dougherty, M. Kurkowiak, N. T. Loges, C. P. Diggle, N. F. Morante, G. C. Gabriel, K. L. Lemke, Y. Li, P. Pennekamp, T. Menchen, F. Konert, J. K. Marthin, D. A. Mans, S. J. Letteboer, C. Werner, T. Burgoyne, C. Westermann, A. Rutman, I. M. Carr, C. O'Callaghan, E. Moya, E. M. Chung, UK10K Consortium, E. Sheridan, K. G. Nielsen, R. Roepman, K. Bartscherer, R. D. Burdine, C. W. Lo, H. Omran, H. M. Mitchison, *CCDC151* mutations cause primary ciliary dyskinesia by disruption of the outer dynein arm docking complex formation. *Am. J. Hum. Genet.* **95**, 257–274 (2014). Medline doi:10.1016/j.ajhg.2014.08.005

22. A. Tarkar, N. T. Loges, C. E. Slagle, R. Francis, G. W. Dougherty, J. V. Tamayo, B. Shook, M. Cantino, D. Schwartz, C. Jahnke, H. Olbrich, C. Werner, J. Raidt, P. Pennekamp, M. Abouhamed, R. Hjeij, G. Köhler, M. Griese, Y. Li, K. Lemke, N. Klena, X. Liu, G.

Gabriel, K. Tobita, M. Jaspers, L. C. Morgan, A. J. Shapiro, S. J. Letteboer, D. A. Mans, J. L. Carson, M. W. Leigh, W. E. Wolf, S. Chen, J. S. Lucas, A. Onoufriadis, V. Plagnol, M. Schmidts, K. Boldt, UK10K, R. Roepman, M. A. Zariwala, C. W. Lo, H. M. Mitchison, M. R. Knowles, R. D. Burdine, J. J. Loturco, H. Omran, DYX1C1 is required for axonemal dynein assembly and ciliary motility. *Nat. Genet.* **45**, 995–1003 (2013). Medline doi:10.1038/ng.2707

23. C. Austin-Tse, J. Halbritter, M. A. Zariwala, R. M. Gilberti, H. Y. Gee, N. Hellman, N. Pathak, Y. Liu, J. R. Panizzi, R. S. Patel-King, D. Tritschler, R. Bower, E. O'Toole, J. D. Porath, T. W. Hurd, M. Chaki, K. A. Diaz, S. Kohl, S. Lovric, D. Y. Hwang, D. A. Braun, M. Schueler, R. Airik, E. A. Otto, M. W. Leigh, P. G. Noone, J. L. Carson, S. D. Davis, J. E. Pittman, T. W. Ferkol, J. J. Atkinson, K. N. Olivier, S. D. Sagel, S. D. Dell, M. Rosenfeld, C. E. Milla, N. T. Loges, H. Omran, M. E. Porter, S. M. King, M. R. Knowles, I. A. Drummond, F. Hildebrandt, Zebrafish ciliopathy screen plus human mutational analysis identifies *C21orf59* and *CCDC65* defects as causing primary ciliary dyskinesia. *Am. J. Hum. Genet.* **93**, 672–686 (2013). Medline doi:10.1016/j.ajhg.2013.08.015

24. K. M. Jaffe, D. T. Grimes, J. Schottenfeld-Roames, M. E. Werner, T. S. Ku, S. K. Kim, J. L. Pelliccia, N. F. Morante, B. J. Mitchell, R. D. Burdine, *c21orf59/kurly* controls both cilia motility and polarization. *Cell Rep.* **14**, 1841–1849 (2016). Medline doi:10.1016/j.celrep.2016.01.069

25. A. Chuma, H. Kitahara, S. Minami, S. Goto, M. Takaso, H. Moriya, Structural scoliosis model in dogs with experimentally induced syringomyelia. *Spine* **22**, 589–594, discussion 595 (1997). Medline doi:10.1097/00007632-199703150-00002

26. M. Turgut, E. Cullu, A. Uysal, M. E. Yurtseven, B. Alparslan, Chronic changes in cerebrospinal fluid pathways produced by subarachnoid kaolin injection and experimental spinal cord trauma in the rabbit: Their relationship with the development of spinal deformity. *Neurosurg. Rev.* **28**, 289–297 (2005). Medline doi:10.1007/s10143-005-0391-8

27. T. H. Milhorat, M. W. Chou, E. M. Trinidad, R. W. Kula, M. Mandell, C. Wolpert, M. C. Speer, Chiari I malformation redefined: Clinical and radiographic findings for 364 symptomatic patients. *Neurosurgery* **44**, 1005–1017 (1999). Medline doi:10.1097/00006123-199905000-00042

28. R. A. Ozerdemoglu, F. Denis, E. E. Transfeldt, Scoliosis associated with syringomyelia: Clinical and radiologic correlation. *Spine* **28**, 1410–1417 (2003). Medline doi:10.1097/01.BRS.0000067117.07325.86

29. M. Verhoef, H. A. Barf, M. W. Post, F. W. van Asbeck, R. H. Gooskens, A. J. Prevo, Secondary impairments in young adults with spina bifida. *Dev. Med. Child Neurol.* **46**, 420–427 (2004). Medline doi:10.1017/S0012162204000684

30. C. M. Karner, F. Long, L. Solnica-Krezel, K. R. Monk, R. S. Gray, *Gpr126/Adgrg6* deletion in cartilage models idiopathic scoliosis and pectus excavatum in mice. *Hum. Mol. Genet.* **24**, 4365–4373 (2015). Medline doi:10.1093/hmg/ddv170

31. C. B. Kimmel, W. W. Ballard, S. R. Kimmel, B. Ullmann, T. F. Schilling, Stages of embryonic development of the zebrafish. *Dev. Dyn.* **203**, 253–310 (1995). Medline doi:10.1002/aja.1002030302

32. K. M. Kwan, E. Fujimoto, C. Grabher, B. D. Mangum, M. E. Hardy, D. S. Campbell, J. M. Parant, H. J. Yost, J. P. Kanki, C. B. Chien, The Tol2kit: A multisite gateway-based construction kit for Tol2 transposon transgenesis constructs. *Dev. Dyn.* **236**, 3088–3099 (2007). Medline doi:10.1002/dvdy.21343

33. L. E. Jao, S. R. Wente, W. Chen, Efficient multiplex biallelic zebrafish genome editing using a CRISPR nuclease system. *Proc. Natl. Acad. Sci. U.S.A.* **110**, 13904–13909 (2013). Medline doi:10.1073/pnas.1308335110